AIP | The Journal of Chemical Physics

Structural and vibrational study of 2-MethoxyEthylAmmonium Nitrate (2-OMeEAN): Interpretation of experimental results with ab initio molecular dynamics

M. Campetella, D. Bovi, R. Caminiti, L. Guidoni, L. Bencivenni, and L. Gontrani

Citation: The Journal of Chemical Physics **145**, 024507 (2016); doi: 10.1063/1.4956459
View online: http://dx.doi.org/10.1063/1.4956459
View Table of Contents: http://scitation.aip.org/content/aip/journal/jcp/145/2?ver=pdfcov
Published by the AIP Publishing

Structural and vibrational study of 2-MethoxyEthylAmmonium Nitrate (2-OMeEAN): Interpretation of experimental results with *ab initio* molecular dynamics

M. Campetella,[1] D. Bovi,[2] R. Caminiti,[1] L. Guidoni,[3] L. Bencivenni,[1] and L. Gontrani[1,a)]
[1]*Dipartimento di Chimica, Università di Roma, "La Sapienza," P. le Aldo Moro 5, I-00185 Roma, Italy*
[2]*Dipartimento di Fisica, Università di Roma, "La Sapienza," P. le Aldo Moro 5, I-00185 Roma, Italy*
[3]*Dipartimento di Scienze Fisiche e Chimiche, Università degli Studi dell'Aquila, Via Vetoio, Coppito, I-67100 L'Aquila, Italy*

(Received 19 March 2016; accepted 27 June 2016; published online 14 July 2016)

In this work we report an analysis of the bulk phase of 2-methoxyethylammonium nitrate based on *ab initio* molecular dynamics. The structural and dynamical features of the ionic liquid have been characterized and the computational findings have been compared with the experimental X-ray diffraction patterns, with infrared spectroscopy data, and with the results obtained from molecular dynamics simulations. The experimental infrared spectrum was interpreted with the support of calculated vibrational density of states as well as harmonic frequency calculations of selected gas phase clusters. Particular attention was addressed to the high frequency region of the cation ($\omega > 2000$ cm^{-1}), where the vibrational motions involve the NH_3+ group responsible for hydrogen bond formation, and to the frequency range 1200-1400 cm^{-1} where the antisymmetric stretching mode (ν_3) of nitrate is found. Its multiple absorption lines in the liquid arise from the removal of the degeneracy present in the D_{3h} symmetry of the isolated ion. Our *ab initio* molecular dynamics leads to a rationalization of the frequency shifts and splittings, which are inextricably related to the structural modifications induced by a hydrogen bonding environment. The DFT calculations lead to an inhomogeneous environment. *Published by AIP Publishing.* [http://dx.doi.org/10.1063/1.4956459]

I. INTRODUCTION

Ionic liquids (ILs) are a class of useful and interesting materials in our fast-moving world both for a variety of scientific and applicative issues.[1–3] Low vapor pressure[4] and high thermal and chemical stability[5] are their most renowned properties and make them a potential replacement for typically polluting volatile organic solvents, although overall environmental safety of ionic liquids is still disputed. The huge number of potentially available ionic liquids is due to the almost unlimited combinations of cations and anions. For this reason it is possible to obtain materials with highly tunable chemical physical properties. Their peculiar properties stem from the complexity of the nanoscopic interactions between their molecular constituents including both long-range Coulombic and short-range van der Waals forces. Several general reviews on this issue have been recently published (e.g., Ref. 6). In addition, many ionic liquids are also characterized by the presence of strong hydrogen bonds.[7,8] An interesting subset of ionic liquids are protic ionic liquids that can be synthesized by combining Brønsted acids and bases.[9] The proton transfer that takes place from the acid (proton donor) to the base (proton acceptor) leads to the formation of a pure liquid consisting of ionic couples where proton acceptor and donor sites eventually generate extended hydrogen-bonded networks,[10–13] largely responsible for molecular aggregation of the condensed phase. In this study we focus on 2-Methoxyethylammonium nitrate (2-OMeEAN, see Fig. 1), a n-alkylammonium salt, where strong hydrogen bonds are established between the N–H$^+$ donor and the $^-$O–N acceptor groups. The interaction gives origin to distinct X-Ray diffraction patterns, already described as regards the low-Q peaks,[14] and to infrared spectra where the bands arising from the donor and acceptor vibrations undergo very large shifts, as reported here for the first time. The infrared spectral patterns are interpreted with the aid of *ab initio* molecular dynamics (AIMD) trajectories, and we show that the same simulation results also reproduce very well the X-Ray patterns already reported. A significant part of this report will include the detailed analysis of the modifications of nitrate group vibrations in this ionic liquid.

In this regard, it is well known[15] that the free anion has a planar structure with the D_{3h} symmetry and that its six normal modes are the totally symmetric stretching (ν_1, A_1'), the asymmetric stretching (ν_3, E_1'), the in-plane deformation (ν_4, E_2'), these last two are doubly degenerate, and the out-of-plane deformation (ν_2, A_2''). A recent work[16] about nitrate in the liquid phase has shown the effects of symmetry breaking on the vibrations of the anion when point symmetry reduces from D_{3h} to C_{2v} up to C_s. The band due to the ν_3 mode of the anion splits into its components and has a broad shape when measurements are made in a polar solvent. Occurrence of hydrogen bonds in the liquid is also responsible for the large broadening of the N–H stretching band.[17] In addition to this aspect, it has been speculated[18] how hydrogen bonds might be a valuable source of disorder in the condensed state

a)Electronic mail: lorenzo.gontrani@uniroma1.it

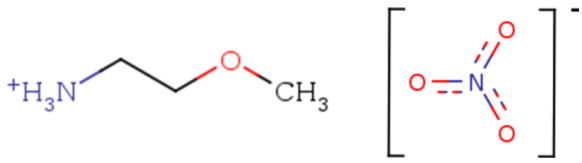

FIG. 1. Sketch of cation and anion for 2-OMeEAN.

of ionic liquids.[11] For example, it has been shown by Kirchner and coworkers[19] by *ab initio* MD (AIMD) calculations that the hydrogen bond network of methylammonium-nitrate is not completely saturated, as roughly just two of the three oxygen atoms of the nitrate form strong bonds. This might be the consequence of strong polarization and many body effects. Owing to the strong dependence of structural and dynamical observables such as radial distribution functions (RDFs) and velocity autocorrelation functions (VAFs) on such effects, it is extremely difficult to obtain valuable computational results using a pairwise potential like that currently employed by classical MD simulations. In this view we propose in this paper an *ab initio* molecular dynamics study in order to interpret the structure of the corresponding bulk liquid system through a detailed analysis of the H-bonding network. In order to provide an interpretation of the measured infrared spectra of the bulk liquid, we have calculated the vibrational density of states (VDOS) by means of Fourier transformation (FT) of the velocity autocorrelation functions. To assign the vibrational properties to specific features of the nitrate distortion and H-bonding we have carried out a detailed analysis of trajectory frames in terms of electronic and geometrical descriptors. Such analysis attributes the degeneracy loss of the nitrate anion asymmetric stretching to the inhomogeneous environment experienced by the anions.

II. EXPERIMENTAL AND THEORETICAL METHODS

A. X-ray diffraction

The large angle X-ray scattering experiments were performed at room temperature using the prototype energy-scanning diffractometer located at the Department of Chemistry at the University "La Sapienza" of Rome (Italian Patent No. 01126484-23 June, 1993). An extended survey of the instrument, the technique, and the experimental protocol of the data acquisition phase can be found in the Refs. 20–22. In this experiment, the $0-2\theta$ instrument geometry (with only one mobile diffractometer arm) was employed; the samples were prepared and put in 2-mm quartz cylindrical capillaries, immediately after a 72-h drying in a high vacuum pump. This setup allows us to record higher diffracted intensities. The diffraction patterns measured at the different angles were then joined into a continuous spectrum in Q; only five diffraction angles are needed to cover a Q-spectrum ranging from 0.1 to 19.56 $Å^{-1}$. The total intensity of the radiation scattered by the sample is corrected for systematic effects (polarization, absorption, and incoherent scattering) and rescaled to absolute units (electron units per stoichiometric unit); it can be expressed as the sum of two terms,

$$I_{EXP}(Q)_{E.U.} = \sum_{i=1}^{N} x_i f_i^2 + I(Q). \quad (1)$$

The first term represents the independent atomic scattering from the atoms in a stoichiometric unit, while I(Q) is the "total (static) structure factor" and contains the structurally sensitive part of the scattering intensity, which is due to the interference contributions from different atoms. The "scattering variable" Q is the magnitude of the transferred momentum and depends on the scattering angle (2θ), according to the relation $Q = \frac{4\pi}{\lambda}\sin(\theta)$, which is equal to $Q \approx 1.0136\ E \sin\theta$, if E is expressed in keV and Q in $Å^{-1}$. The function I(Q) is related to the pair correlation functions descriptive of the structure, according to the following formula:

$$I(Q) = \sum_{i=1}^{N}\sum_{j=1}^{N} x_i x_j f_i f_j \times \left[4\pi\rho_0 \int_0^{\infty} r^2(g_{ij}(r)-1)\frac{sinQr}{Qr}dr\right], \quad (2)$$

where ρ_0 is the bulk number density of the system, x_i are the numerical concentrations of the species, and f_i their Q-dependent X-ray scattering factors.

Both the experimental and theoretical structure functions were multiplied by a modification function

$$M(Q) = \frac{f_N^2(0)}{f_N^2(Q)}\exp^{-0.01Q^2} \quad (3)$$

to improve the curve resolution at high Q, and then Fourier-transformed into the "Differential radial distribution function" (Diff(r)) which contains only the structural contribution to the distribution function, according to the relation

$$Diff(r) = \frac{2r}{\pi}\int_0^{\infty} QI(Q)M(Q)sin(Qr)dQ. \quad (4)$$

Summarizing, the comparison between experimental and model data is carried out using both QI(Q)M(Q) and Diff(r), while for the discussion of the model characteristics we will use both the partial correlation functions $g_{ij}(r)$ and the total Diff(r). All the above functions were calculated from MD trajectories using g_rdf (Gromacs suite[23]) and *in-house* codes purposely written.

B. IR measurements

The Fourier transform infrared (FTIR) measurements were performed with a Bruker 66V FTIR spectrometer. We measured the transmittance spectra from the Far-IR (FIR) to the Mid-IR (MIR) (30-5000 cm^{-1}). For the FIR region we used a Mylar beamsplitter and a room temperature DLATGS (deuterated L-alanine doped triglycine sulphate) detector. The MIR region was investigated through a potassium bromide beam splitter and a Mercury Cadmium Tellurium (MCT) detector working at 77 K.

A Bruker cell equipped with zinc telluride (ZnTe) and polyethylene windows having a variable path length from 0.020 to 0.010 mm was used for the IR measurements in transmission. The cell was positioned in the sample compartment of the interferometer in the focus of an f/4 parabolic mirror and

the transmitted beam was collected by a twin mirror and then focused onto the detector. The empty cell was used as reference in the measurements and the transmittance $T(\nu)$ (where ω is the frequency in cm^{-1}) has been calculated as $T(\omega) = I(\omega)/I_0(\omega)$, where $I_0(\omega)$ ($I(\omega)$) is the intensity transmitted by the empty (filled with the ionic liquid) cell. Finally, for each spectrum 128 scans were recorded at a spectral resolution of 4 cm^{-1}.

C. Computational details

To investigate the structure and vibrational spectra of 2-methoxyethylammonium we studied a bulk system composed of 32 ion pairs. Before the Quantum Mechanical (QM) calculation, the system was pre-equilibrated at 300 K with a 2 ns classical molecular dynamics NPT simulation, using the AMBER[24] program package and the Gaff[25,26] force field. The difference between MD and experimental densities was within 5%; the edge of the cubic box corresponding to the density value was approximately 18.4 Å. The final configurations that resulted from this procedure were used to set up the *ab initio* simulation, which was run with the program package CP2k,[27] using the Quickstep module[28] and orbital transformation[29] for faster convergence. The electronic structure was calculated with density functional theory,[30,31] using the Perdew–Burke–Ernzerhof (PBE)[32] functional, with explicit van der Waals terms that include the empirical dispersion correction (D3) by Grimme.[33] Molecularly Optimized Short Range Goedecker Teter Hutter (GTH)[34] basis sets and GTH pseudopotentials[35,36] were employed. The time step chosen was 0.5 fs and the temperature was set at 350 K by a Nóse-Hoover chain thermostat. After 7 ps of QM equilibration, a 46 ps *NVT* trajectory was produced. During the simulation the Wannier centers of the whole system, with a print frequency of one every five steps, were computed to allow us to obtain the relative theoretical infrared spectra. Another set of static *ab initio* calculations was carried out on the individual NO_3^- and $CH_3OCH_2CH_2NH_3^+$ ions, ion pairs, and small clusters (up to ten ion pairs) using the Gaussian program,[37] employing both the hybrid functional B3LYP[38] and the dispersion-corrected wB97XD functional,[39] with the 6-311++G(3df,3pd) basis set. In detail, geometry optimizations and harmonic frequencies calculations were computed to determine the respective *in vacuo* infrared spectra; analogous calculations were also run within the Polarized Continuum Model (PCM) approximation[40] to take into account the effect of different surroundings (chosen on the ground of dielectric constant values) on the vibrational spectrum of each component of the ionic-couple. The PCM simulations were based upon the following dielectric constants: 78.355 (water), 24.852 (ethanol), 1.882 (n-hexane), 1.706 (xenon), 108.94 (formamide), and 26.3 (ethylammonium nitrate). All these calculations were accomplished to test the performance of the computational methods in the determination of the vibrational frequencies of the uncoordinated ionic fragments and of the ion pair.

D. Vibrational analysis

The vibrational density of states (VDOS) can be obtained directly using *ab initio* MD by calculating the Fourier transform of the velocity autocorrelation function,

$$P(\omega) = \sum_{i=1}^{N} \int_{-\infty}^{+\infty} dt \langle \vec{r}_i(t) \cdot \vec{r}_i(t) \rangle \exp(i\omega t) = \sum_{i=1}^{N} P_i^r(\omega) = \sum_{i=1}^{3N-6} P_k^q(\omega), \quad (5)$$

where $P_i^r(\omega)$ is the VDOS for the i-th atom of the system (N is the total number of atoms) with position $\vec{r}_i(t)$. Recently, the concept of normal mode analysis has been extended to a finite temperature formulation,[41,42] introducing a linear transformation from the internal variable of the molecule (3N-6) to a generalized coordinate q_k. The total VDOS $P(\omega)$ can be therefore decomposed into a sum of (3N-6) spectral terms, P_k^q (partial VDOS of the transformed coordinate q_k, Eq. (5)), obtained by minimizing the functional $\Omega^{(n)}$ (Eq. (6)) with respect to the chosen set $\{q\}$

$$\Omega^{(n)} = \sum_k \left[\frac{\beta}{2\pi} \int_{-\infty}^{+\infty} d\omega |\omega^{2n}| P_k^q(\omega) - \left(\frac{\beta}{2\pi} \int_{-\infty}^{+\infty} d\omega |\omega^n| P_k^q(\omega) \right)^2 \right]. \quad (6)$$

The obtained set of the coordinates q_k, referred as effective normal modes, describe the collective motions characterized by a single peak shape around the frequency ω_k. The term "effective" means that the final normal modes extracted from this procedure take into account the finite temperature of the dynamics, the configurational averaging, the presence of the solvent, and vibrational anharmonicity effects. In Eq. (6) we used the standard value $n = 2$ that allows us to replace the minimization problem by a generalized eigenvalue problem. This technique has been recently applied with success to dissect the vibrational spectra of liquids and biomolecules in solution. The IR spectrum $I_{IR}(\omega)$, i.e., band-positions, shapes, and intensities, can be also obtained directly through the Fourier transformation of the dipole auto-correlation function,

$$I_{IR}(\omega) = \frac{2\pi\beta\omega^2}{3cV} \int_{-\infty}^{+\infty} dt \langle D(t)D(0) \exp(i\omega t) \rangle. \quad (7)$$

III. RESULTS

A. X-ray patterns

The comparison between the theoretical structure factor and the corresponding experimental measurements[43–48] of 2-OMeEAN is the first results to be considered. The experimental data taken into account have already been reported in a previous work.[49]

Figure 2 shows the QI(Q)M(Q) function in the upper panel and the Diff(r) functions obtained by Fourier transformation of the same data in the lower panel. From a qualitative analysis of the structure factor curve, we can point out the presence of a principal peak falling at 1.68 $Å^{-1}$, the presence of two smaller peaks—resembling shoulders—at 2.54 and 4.28 $Å^{-1}$, and the absence of a pre-peak. As explained in a previous work by some of us,[49] the occurrence of a low-Q peak in the simulated pattern can be ascribed to the overwhelming

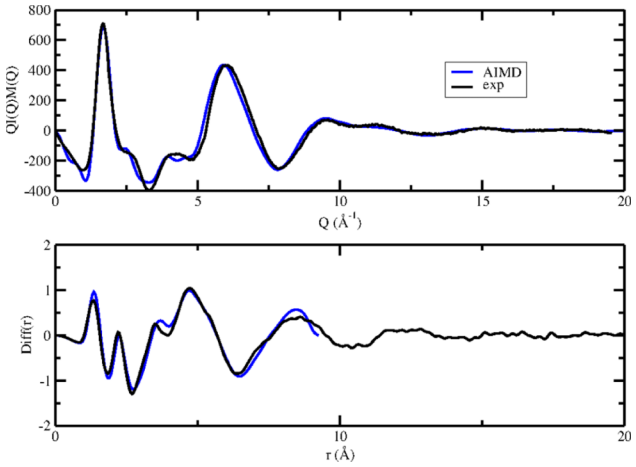

FIG. 2. Upper panel: 2-OMeEAN QI(Q)M(Q) experiments and theory. Lower panel: Fourier transform of the above data, Diff(r).

presence of the extended or *anti* conformer in the structure of the liquid yielded by classical MD calculations. In the configurations sampled, in fact, the cations can be clustered into two main conformations differing by the NCCO dihedral angle value: 60° (*gauche*, bent) and 180° (*anti*, extended). The presence of a certain amount of *gauche* conformers prevents the interaction between alkyl chains and the consequent formation of the pre-peak. For this reason, to be able to assess the relative percentage of *anti* and *gauche* conformers in the liquid, the intramolecular RDF related to the N···O distance and the Dihedral Distribution Function (DDF) of the torsional NCCO angle were calculated. The DDFs are shown in the supplementary material. The RDF shows two peaks, at 2.9 Å and 3.7 Å; the first peak is associated with the formation of a hydrogen bond between the two ends of the chain,[49] while the second peak is related to an open conformation. The relative weights of the two peaks are 3:1 and in this way the *gauche* population suggested by *ab initio* molecular dynamics is about 2.5 times greater than the classical MD result, obtained using the point charges of the gauche form (see Fig. 6 of Ref. 49). This finding verifies the medium-long range order breaking due to the presence of an heteroatom in the alkyl chain.[14,50] In the radial pattern (lower panel of Fig. 2), the first two peaks are related to first and second neighbour contacts (1-2 and 1-3) within the molecules, whereas in the range 2.7–6 Å both long intramolecular correlations (head-to-tail contacts) as well as intermolecular cation-anion hydrogen bond interactions contribute. The strongest interactions give origin to the peaks falling at 3.5 and 4.7 Å and to the shoulder around 6 Å. Further on, the structural correlations fades out, the last visible oscillation occurring at about 10.2 Å.

Considering the comparison between the simulated and theoretical patterns, there is good agreement in the whole range both in QI(Q)M(Q) and Diff(r) functions, apart from a small overestimation of the hydrogen bond interaction at 2.95 Å due to N···O contacts between ammonium and nitrate, which is too intense. Moreover, the theoretical Diff(r) terminates earlier than the experimental one, because of the limited extension of the simulation box allowed by the available computational resources. The edge box, in fact, is about 18.4 Å and accordingly, the periodic boundary conditions impose a 9.2 Å limit (half box edge) to the explorable distances. As noted above, the last experimental peak ends at about 10.2 Å, so we can state that the entire range of the pair distances having appreciable contribution to the Diff(r) could be spanned.

After validating the simulation, we were able to use the trajectory to gather structural information. The simplest geometric information that can be extracted is the radial distribution function g(r). Despite its simplicity, this is a crucial feature because the Fourier transform of all g(r)'s yields the total scattering functions[51] that can be actually measured (see Equations (2)-(4)). The radial distribution functions between several representative atoms of the cation(2-OMeEA) and nitrate anion are shown in Fig. 3.

The black line appearing in Fig. 3 refers to the RDF of N(OMeEAN)···O(Nit). It shows two distinctive peaks at 2.8 Å and 4.6 Å: the first peak is clearly due to direct hydrogen bond interaction between the heteroatoms, while the second one derives from the other two oxygen atoms of the nitrate anion indirectly coordinated to the ammonium group of the cation. The location of the these peaks is in good agreement with the results of previous works.

In the same picture, the RDF between the two nitrogen atoms of the nitrate anions is shown in red, while the RDF between the alkyl chains of cations is represented in blue. No clear ordering could be observed in both the RDFs as the first RDF shows a broad peak at about 5.4 Å and the second one is rather featureless, suggesting thus the absence of direct interaction between the nitrate anions or the alkyl chains. However, there is an effect of indirect coordination due to direct anion-cation interaction.

In order to provide three dimensional information about the relative distribution of the anions, we report in Fig. 4 several Spatial Distribution Functions (SDFs).[52]

In each plot the isosurface has been drawn so as to include half of the density. As it can be noted, the oxygen atoms of the anions in the first solvation shell around the cation (red line) are mainly localized around the NH_3^+ group, with the H-bond distance (acidic hydrogen–oxygen) sweeping a narrow circular cone by rotation around the N–H bond. As shown in the left side of Fig. 4, the second solvation shell

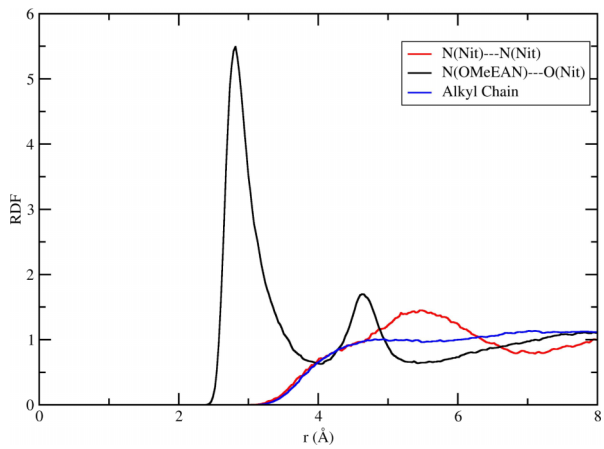

FIG. 3. Black: RDF between N(2-OMeEA) and N(Nit); red: RDF between nitrate atoms of anions; and blue: RDF between alkyl chains of cations.

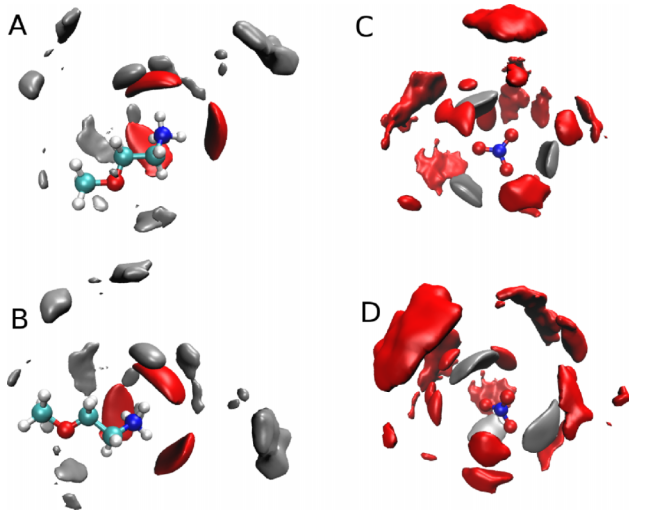

FIG. 4. Left: SDF of the oxygen atoms of anions (red) and the alkyl chain of cations (grey) around the cation. Right: SDF of the nitrogen atom of the cation (grey) and Center Of Mass (c.o.m.) of the anion (red) around the anions. The difference between the upper and lower pictures is only the point of view.

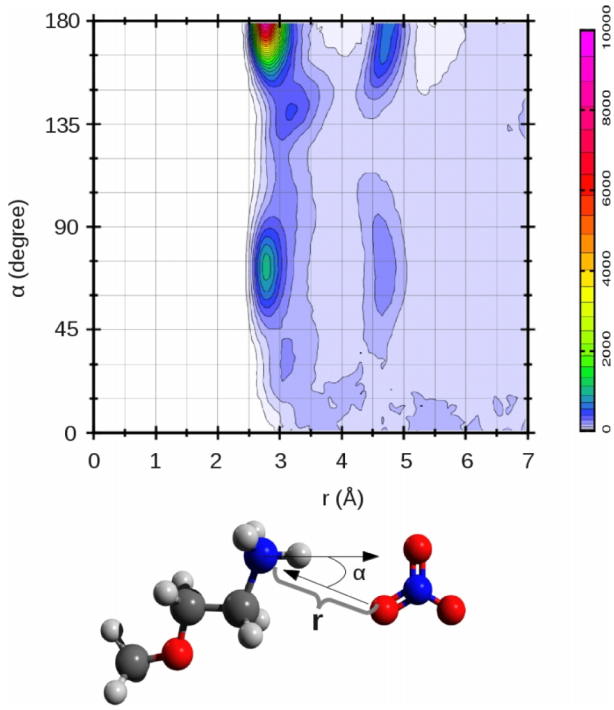

FIG. 5. Combined distribution function showing the hydrogen bond between anions and cations.

around the cation was calculated by sampling the cation alkyl chain (grey line). This shell is less structured and is preferably localized around the ammonium group. In this bulk phase, the typical geometrical arrangement characterized by alternating patterns of the cation and anion can be observed. The geometrical distribution around the anion is also shown in Fig. 4 on the right side. The nitrogen atom of the cation in the first shell (grey line) has a trigonal shape around the anion. The asymmetry of the hydrogen bond network already noticed in Ref. 19 is here suggested once again by the lower density of one of the three lobes of the surface that it is due to a reduced ability of the anion to form a third hydrogen bond together with the remaining two. Even in this case one can see patterns of alternating cations and anions. To better characterize the cation-anion interaction, the relative Combined Distribution Function (CDF) was calculated.[53] The CDF distribution correlates the N(2-OMeEA)$\cdots$N(Nit) distance and the distribution of the angle between the two vectors, the first is the NH^+ bond and the second connects the heteroatoms involved in the hydrogen bond (N and O). The corresponding function is shown in Fig. 5.

This figure shows a tall peak with maximum at about 2.8 Å/180°; both distance and angle values satisfy the criteria for classifying such interaction as an hydrogen bond. A further analysis of the effect of the hydrogen bond network established in the system, focusing in particular upon the asymmetric environments experienced by the ions, regarded the experimental IR spectrum, which was interpreted by means of the Vibrational Density of States (VDOS) calculated from the *ab initio* trajectory.

B. AIMD analysis of IR spectrum

The comparison between AIMD and experimental IR spectra is shown in Fig. 6, upper panel; the calculated spectrum was itemized into its cationic and anionic components in the bottom panel. The simulated spectrum is in satisfactory agreement in all the frequency range, confirming the reliability of our model. Moreover, the analysis of the separate contributions points out that at high frequency, the major contribution to the spectrum comes from the cation, whereas the most prominent peak occurring around 1350 cm^{-1} arises mostly from anion vibrations.

It is of valuable interest that the intensity, position, and broadening of the peaks are well reproduced by the theoretical model. The assignment of each peak was performed using the MOLSIM package.[54,55] For this purpose, a set of internal coordinates[56] was defined and subsequently the Fourier transform of the velocity autocorrelation of all atoms was calculated and projected onto the effective normal modes (built as a suitable linear combination of internal coordinates). It should be kept in mind that following this

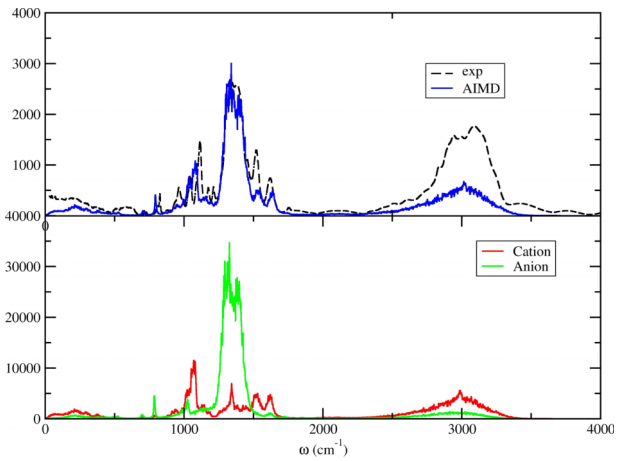

FIG. 6. Experimental vs. theoretical IR spectra.

procedure, the autocorrelation function of the atom velocities is considered and therefore all the vibrational modes of the system, independently of their IR or Raman activity, are computed. In the following, the effective normal modes having direct comparison with experimental infrared spectrum and an appreciable contribution in the partial spectrum are examined (see the lower panel of Fig. 6). For the sake of clarity, the vibrational analysis of the cation and anion is discussed separately. The results of this simulation are reported in Table I along with the comparison with the experimental data. The region from 800 cm^{-1} to 1800 cm^{-1} was chosen for the discussion because the normal modes occurring in this frequency range represent the "fingerprint" of the ion-couple and are indirectly affected by hydrogen bond interactions.

Regarding the higher frequency range ($\omega > 2000$ cm^{-1}), a quite broad band is observed in both experimental and simulated spectra. The origin of this feature is mostly due to the superposition of the CH and NH stretching vibrations. The broadening can also be due to possible overtones and combination bands having weak IR intensity.[57] Whereas the CH stretchings are highly localized, i.e., their distribution functions are rather narrow, NH vibrations are distributed over a wide frequency range (3100-3400 cm^{-1}), owing to the strong hydrogen bonds that N–H fragments establish with the anions, as found for other protic ionic liquids.[17] Despite its lower degree of complexity, the study of the anion vibrations is very interesting because they are directly involved in fingerprints of the hydrogen bond network of the complex. The most typical feature of the spectrum is the intense and relatively broad peak spanning from 1250 to 1500 cm^{-1} and it is mostly related to N–O stretchings. Remarkably, the shape and thickness of the experimental spectrum are closely reproduced by the calculated pattern. The absorption peaks observed, which will be assigned in detail later in this work, are significantly broadened by the inhomogeneous environment, as suggested by the analysis of the AIMD trajectory. As a matter of fact, the nitrate anion has three different anchor points (the oxygen atoms) that are hydrogen bond acceptors and may coordinate several cations around themselves forming one or more hydrogen bonds in the liquid phase. This heterogeneous *ensemble* of different configurations is responsible for slightly different frequencies. Some representative structures are shown in Fig. 7.

To investigate the details of the environmental effect, we have analyzed the properties of each nitrate anion along the trajectory. From the analysis, the environment around each anion turned out to be highly heterogeneous in terms of hydrogen bond patterns and local distribution of counterions. This heterogeneity has a strong effect on the electronic properties of the anion and on its vibrational spectrum. Among all the possible spatial arrangements, we were able to identify some representative categories into which the different anions could be grouped. For every kind of anion(s), we have first calculated the RDF between the nitrogen atoms of the cation and anion, as well as between the nitrogen atom of the anion and the methoxyl carbon of the cation. Also the hydrogen bond population, total dipole distribution function, the NO length distribution function, the dipole projections along the bond NO axis distribution function and the Fourier transform of the velocity, and dipole autocorrelation function in the ν_3 ω region are of the key points of this analysis. The analysis of the trajectory revealed that five qualitatively different cases coexist in the liquid phase along the dynamics, as reported in Fig. 8. The anion molecules with a similar chemical environment, therefore sharing common features in terms of properties, were therefore assigned to one of these five groups. In the graphs, the colors in the dipole projection distribution function and in the NO bond length distribution function are referred to the same NO bond. The remaining three normal

TABLE I. Assignment of the vibrational modes and experimental IR frequencies in the $800 < \omega < 1800$ cm^{-1} range. Values are in wavenumbers (cm^{-1}).

Molecule	Expt. frequency	AIMD	Mode
Anion	720	725-708	In-plane bend (ν_4)
Anion	825	799	Out-of-plane bend (ν_2)
Anion	1046	1042	Symm str ($\nu 1$)
Anion	1336	1353	Asymm str (ν_{3a})
Anion	1382	1408	Asymm str (ν_{3b})
Cation	808	857	HCCH tors
Cation	883	907	HCCC/HCCH tors
Cation		955	HNCC/HCOC tors
Cation	964	933	CC/CN str
Cation	1027	997	CN/CO str
Cation	1088	1044	CC/CN/CC str
Cation	1116	1089	HNCC tors
Cation	1175	1151	CO str
Cation	1213	1164	CO str/CH_3 bend
Cation	1275	1284	HCN bend
Cation	1457	1531	CH_3/CH_2 bend
Cation	1480	1451	CH_3 bend
Cation	1521	1467	NH_3^+ bend
Cation	1621	1628	NH_3^+ bend
Cation		1638	NH_3^+ bend

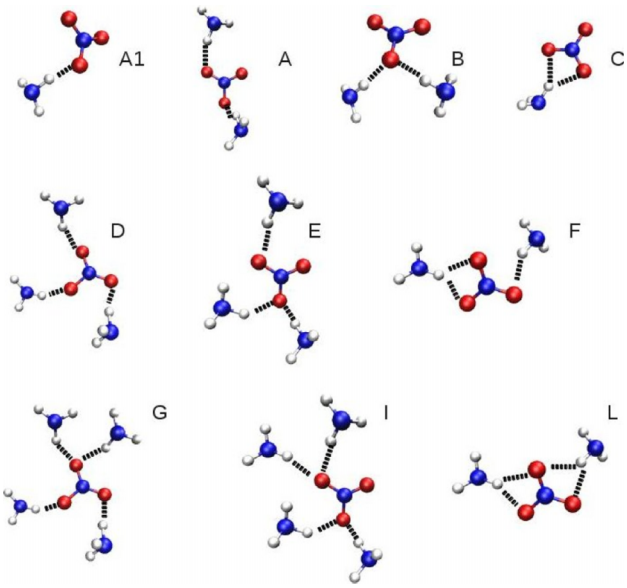

FIG. 7. Representative structures of the H-bond pattern.

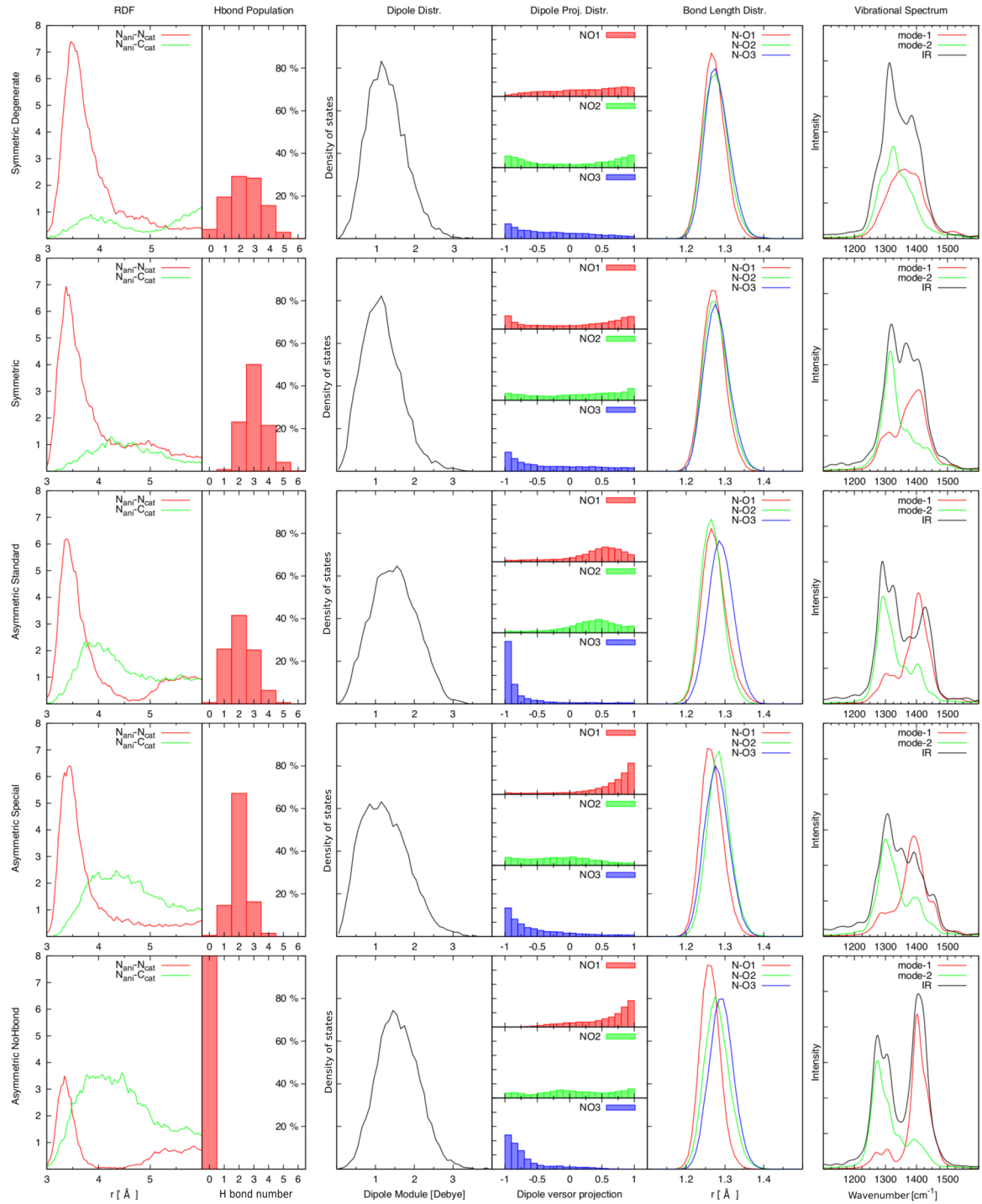

FIG. 8. Analysis of electronic, geometrical, and vibrational properties of five different groups of nitrate anions along AIMD simulations.

modes of the anion, namely the in-plane deformation (ν_4), which would preserve apparent degeneration notwithstanding symmetry lowering, the out-of-plane deformation (ν_2), and the symmetric stretching (ν_1), were not taken into account in such analysis because they are scarcely affected by the hydrogen bond network. All these vibrations are environment-independent hence they have the same frequency for all of the possible conformers. The frequencies under consideration are listed in Table I.

From this sampling, qualitatively different environments influencing the properties of the anion were found. The first group of configurations, called "symmetric degenerate," is characterized by the following common features: the RDFs show a stronger coordination with NH_3^+ than with the cation aliphatic moieties. The anions of this cluster explore a number of different hydrogen bond contacts (confirming the strong interaction with the ammonium group suggested by the RDF), although each coordination has the same probability. The total dipole distribution function has a maximum placed at about 1.1 D and its projections show no preferential orientation along the NO bonds. The latter aspect agrees with the bond distribution functions between the nitrogen and oxygen atoms

because the bonds have the same equilibrium value falling at 1.27 Å.

Despite the fact the three oxygens of the nitrate anion are surrounded by the same local chemical environment on average, the VDOS analysis shows a loss of degeneracy in the ν_3 normal mode and a splitting into two different peaks (named as mode 3a and mode 3b), that occur at 1320 cm^{-1} (3a) and 1380 cm^{-1} (3b). Anyway, while all of the three oxygen atoms explore the same average medium, the presence of cation molecules breaks the double degeneration of the ν_3 normal mode, contrary to the ν_4 normal mode. The second group, "symmetric," has features similar to the first group; also in this case all nitrate oxygen atoms are indistinguishable because, on average, they undergo the same intermolecular interaction; the results of this behavior are equivalent bond length and no preferred orientation of dipole moment along the NO bond. The only difference with respect to the symmetric degenerate group is the hydrogen bond population and the prevalent formation of structures bearing three hydrogen bonds, one for each oxygen atom (about 50% of the time). The high occurrence of such conformers leads to a blue shift for the mode ν_{3b} and the red shift for the mode ν_{3a}.

Unlike the previous case, the calculated splitting of the two normal modes is indeed larger, being about 140 cm^{-1}. The next groups can be described as "asymmetric," since the three oxygen atoms behave differently and their spatial distribution is highly unbalanced.

For the first two antisymmetric cases the anions show a well shaped RDF between the nitrogen atoms, and they are involved in hydrogen bonds for 100% of their time. In the first asymmetric case (third group), indicated as "asymmetric standard" in Fig. 8, a hydrogen bond is stronger than the other two; as a result, one N–O bond is more elongated and the total dipole moment is preferentially oriented along this bond (blue pattern). Owing to this asymmetry the normal modes ν_{3a} and ν_{3b} are well separated and also for this type of anion the frequency splitting is about 140 cm^{-1}. In the "asymmetric special" anions (fourth case) to two hydrogen bonds (and two consequent longer N–O bonds) originate the asymmetry of the environment surrounding the anion. The dipole moment tends to lie along such bonds and the resulting VDOS show a large energy difference between the 3a and 3b components of the ν_3 mode. The last group to be considered is the "asymmetric no-hydrogen bond" that includes anions not forming any hydrogen bond during the entire trajectory. The RDFs show a weak coordination of NH^+ and a fair arrangement of the alkyl chain around the anion, while only one structure is present in the hydrogen bond distribution histogram, namely that with zero hydrogen bonds. Despite the lack of participation to the hydrogen bond network, the VDOS function of this configuration exhibits a strong shift due to the different NO bond strengths of the anions, meaning that the long range interactions existing between the cation and anion are not negligible. This issue can be appreciated in the radial distribution function N-anion vs C-cation (green curve), that is significantly above unity. Even if such interactions are weaker than hydrogen bonds, they are still strong enough to induce a significant asymmetry on the nitrate anion, leading to results similar to those seen in the "asymmetric special" case. It should be kept in mind that the former analysis is strictly related to the trajectory sampled. In a longer timespan, the anions could possibly change the class they belong to.

C. Comparison with static *ab initio* analysis

The infrared spectra obtained from *ab initio* molecular dynamics trajectories were compared with those calculated with more "standard" *ab initio* methods. The first step of the computational study regarded the isolated ions, the two forms of the cation (*gauche* and *anti*), and the NO_3^- anion. The hybrid functionals B3LYP[38] and PBE1PBE[58] and the functional wB97XD, which includes Grimme empirical dispersion,[33] were employed, with the 6-311++G(3df,3pd) and the 6-311++G(d,p) basis sets. This procedure was followed in order to assess the quality of the results obtained from different functionals and basis sets in view of more sophisticated and computationally demanding calculations. The use of the less extended 6-311++G(d,p) basis set produces results of comparable quality with respect to the more extended basis set, at least for the vibrational frequencies of each ion. The wB97XD functional was preferred to the others because it incorporates empirical dispersion and therefore all the calculations involving ion-couples were carried out at the wB97XD/6-311++G(d,p) level.

As skillfully explained elsewhere,[59–61] the simulation of the vibrational spectrum of the single ion pair cannot be accomplished *in vacuo* because proton transfer from NH_3^+ to NO_3^- occurs. Another point to be considered for the success of the calculation of the vibrational spectrum is the choice of a properly sized cluster and is endorsed by the splitting of the ν_3 mode of nitrate. In fact, the distribution of the vibrational modes is thoroughly subordinated to the actual interactions between the cationic and anionic groups modeling the whole system. In this study the smallest cluster taken into account consists of two ion-couples and the more complex structures consist of 4, 6, 8, and 10 ion couples. The gradual improvement of these simulations, increasing with the complexity of the model, is due to the fact that a larger and larger number of nitrate anions is almost completely surrounded by NH_3^+ groups and in this way most of the nitrogen-oxygen bonds are somehow equivalent. In this way, a fewer number of nitrogen-oxygen bonds assume the partial double-bond character and the splitting of the ν_3 vibration consequently decreases. One has to remark, though, that even the largest clusters considered, owing to their spatial limit, always show nitrate or ammonium groups not fully coordinated. This leads to the consequence that the distribution of singly/doubly bonded nitrogen-oxygen bond is biased by the choice. For this reason, after a careful analysis of all simulated spectra, it was decided that the model containing ten cations and anions gave the best compromise in terms of accuracy and computational affordability.

The chemical environment experienced by the most of the anions resembles **D** and **G**-type schemes and a reduced amount of nitrates undergoes a coordination with NH_3^+ groups, similar to the **E** and **I**-type schemes of Fig. 7. For the system under consideration, the picture is however much complex because the cation may exist in the *anti* and *gauche* conformations.[49] The most evident feature of

the latter conformer is an intramolecular hydrogen bond. Calculations restricted to the two cationic forms indicate that the two conformers would be distinguishable, at least on the theoretical viewpoint and this makes the study more intricate, even uncertain, when the theoretical findings are employed to investigate the experimental FTIR spectrum. Also in this case, the wB97XD/6-311++G(d,p) infrared spectrum was simulated for the cluster made of 10 ion couples. Both the largest clusters produced by the two different cations and the corresponding infrared spectra are shown in Figure 9. The summary of the proposed assignment of the FTIR spectrum is reported in Table II and the assignment is based on the Potential Energy Distribution (PED) generated by the VEDA software[62] for the individual ionic fragments for the simplest aggregates and more generally using the Molden package[63] through normal mode visualization. The procedure implemented in VEDA generates a set of 3N-6 linearly independent internal coordinates and then optimizes their contribution in the Potential Energy Distribution (PED) matrix.

Relying on the experimental evidence that the strongest infrared bands of the FTIR spectrum are due to the antisymmetric stretching of the anion separated by 46 cm^{-1}, suggesting that coordination around the anion is particularly extended, the amount of the splitting of the ν_3 mode of NO_3^- that is predicted by the calculations has a relevant role in the present analysis.

The most substantial conclusions accomplished from these calculations can be summarized as follows.

The NH and CH vibrations of the high frequency range of the infrared spectrum are distributed as shown in Table II. The NH stretchings are lying over the frequency range spanning from 3500 to 3100 cm^{-1}, indicating a different arrangement of nitrogen-hydrogen bonds in the complex hydrogen-bond network of the cluster. The lowest frequency NH stretching is predicted to lie close to some CH modes. The measured IR spectrum reveals a series of high energy absorptions spanning a wide wavenumber range. Among these bands, those measured at 3435, 3250, and 3150 cm^{-1} have a broad profile, appear as low or medium intensity bands, and are assigned, according to the present and former[59–61] calculations, to the NH stretching vibrations of the complex. All the remaining bands belong to different CH stretchings. The IR band measured at 3150 cm^{-1} should be related to the lowest energy NH stretching, considerably perturbed by coordination with the anion, as also suggested by computations on clusters of closely related ionic liquids.[59–61]

The NH_3^+ group bendings are scarcely affected by complexation, at least with respect to the stretching modes. The calculations predict these vibrations within 1700 and

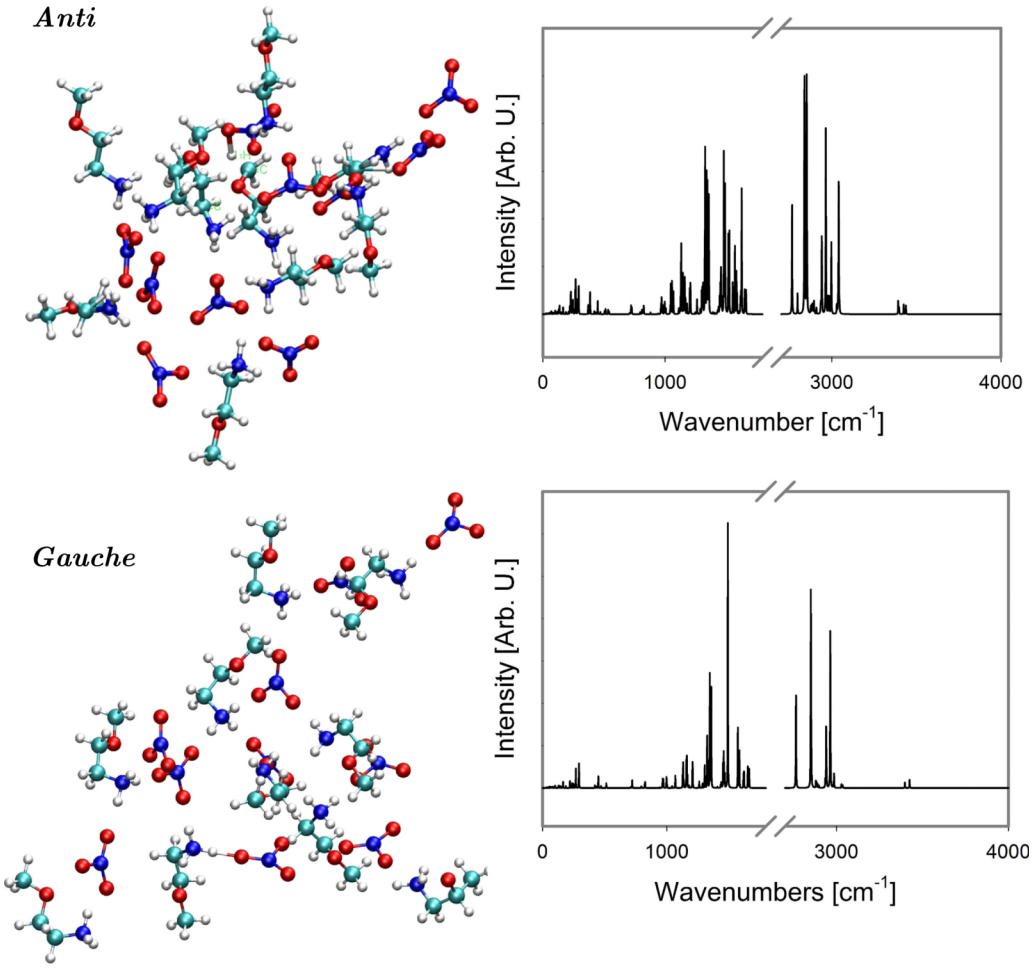

FIG. 9. The ten-atom clusters (left) containing *Anti* and *Gauche* cations, used to calculate the IR spectrum (right).

TABLE II. Calculated and experimental IR frequencies α = near NH_3; β = near OCH_3. Nitrate normal modes in gray.

Gauche	*Anti*	*Gauche*	*Anti*	FTIR (expt.)
3557 ν NH_3^+	3530 ν NH_3^+	3558 ν NH_3^+	3568 ν NH_3^+	3435
3500 ν NH_3^+	3523 ν NH_3^+	3533 ν NH_3^+	3540 ν NH_3^+	3250
3356 ν NH_3^+	3440 ν NH_3^+	3168 ν NH_3^+	3088 ν NH_3^+	3150
3189 ν $CH_2(\alpha)$	3187 ν $CH_2(\alpha)$	3167 ν $CH_2(\alpha)$	3166 ν $CH_2(\alpha)$	3092
3181 ν CH_3	3183 ν CH_3	3158 ν CH_3	3158 ν CH_3	2999
3121 ν $CH_2(\alpha)$	3115 ν $CH_2(\alpha)$	3103 ν $CH_2(\alpha)$	3107 ν $CH_2(\alpha)$	2940
3117 ν CH_3	3097 ν CH_3	3070 ν CH_3	3063 ν CH_3	2988
3078 ν $CH_2(\beta)$	3027 ν $CH_2(\beta)$	3046 ν $CH_2(\beta)$	3020 ν $CH_2(\beta)$	2941
3040 ν CH_3	2990 ν CH_3	3001 ν CH_3	3003 ν CH_3	2934
3010 ν $CH_2(\beta)$	2957 ν $CH_2(\beta)$	2992 ν $CH_2(\beta)$	2972 ν $CH_2(\beta)$	
1682 δ NH_3^+	1672 δ NH_3^+	1713 δ NH_3^+	1728 δ NH_3^+	1621
1653 δ NH_3^+	1671 δ NH_3^+	1651 δ NH_3^+	1688 δ NH_3^+	1521
1515 δ NH_3^+	1534 δ NH_3^+	1572 δ NH_3^+	1644 δ NH_3^+	
1536 δ $CH_2(\beta)/CH_3$	1526 δ $CH_2(\alpha,\beta)/NH_3^+$	1512 δ CH_3	1527 δ $CH_2(\alpha)$	
1506 δ $CH_2(\alpha)/CH_3$	1506 δ $CH_2(\alpha)$	1494 δ CH_3	1499 δ CH_3	1480
1500 δ $CH_2(\alpha,\beta)/CH_3$	1499 δ $CH_3/CH_2(\alpha,\beta)$	1487 δ $CH_3/CH_2(\beta)$	1494 δ $CH_3/CH_2(\beta)$	
1497 δ CH_3	1498 δ CH_3	1509 δ $CH_2(\alpha)$	1493 δ CH_3	
1487 δ CH_3	1493 δ CH_3	1453 δ $CH_2(\alpha,\beta)/CH_3$	1467 δ $CH_3/CH_2(\alpha,\beta)$	1457
1445 δ $CH_2(\alpha,\beta)/CH_3$	1467 δ $CH_3/CH_2(\alpha,\beta)$	1414 δ $CH_2(\alpha,\beta)$	1466 δ $CH_3/CH_2(\alpha,\beta)$	
1404 δ $CH_2(\alpha,\beta)$	1388 δ $CH_2(\alpha,\beta)$	1397 ν_{3a}	1409 ν_{3a}	1382
1356 δ HCN	1345 δ HCN	1384 ν_{3b}	1369 ν_{3b}	1336
1290 δ HCO	1305 δ HCO	1361 δ HCN	1361 δ HCN	1275
1247 ν CO/τ HCOC	1257 ν CO/CH_3	1254 ν CO/CH_3	1258 ν CO/CH_3	1213
1203 τ HCOC	1207 τ HCOC	1213 τ HCOC	1215 τ HCOC	
1178 τ HCOC	1197 ν CO	1188 ν CO	1207 ν CO	1175
1118 τ HNCC	1155 τ HNCC/CC	1159 τ HNCC	1175 τ HNCC	1116
1040 ν CC/CN/CO	1022 ν CC/CN/CO	1089 ν CC/CN/CO	1092 ν CC/CN/CO	1088
		1107 ν_1	1114 ν_1	1046
992 ν CO	982 ν CN/CO	1012 ν CO	1013 ν CN/CO	1027
965 τ HNCC/HCCH	948 τ HNCC/HCCH	918 τ HNCC/HCCH	1005 τ HNCC/HCCH	883
892 ν CC/CN	919 ν CC/CN	917 ν CC/CN	983 ν CC/CN	964
		852 ν_2	858 ν_2	825
816 τ HCOC/HCCO	804 τ HCCH	842 τ HCOC/HCCO	835 τ HCCH	808
		753 ν_{4a}	750 ν_{4a}	
		743 ν_{4b}	740 ν_{4b}	720

1540 cm^{-1} (see Table II). Experimentally, the only observed bands attributable to the deformation modes of ammonium are measured at 1621 and 1521 cm^{-1}. Other NH_3^+ deformation modes having low infrared intensity are computed in the 1300-1400 cm^{-1} range but there is no experimental evidence from the analysis of the FTIR spectrum.

The carbon-carbon, carbon-nitrogen, and carbon-oxygen stretchings are strongly vibrationally coupled among each other. The first two modes are actually described as linear combinations of carbon-carbon and carbon-nitrogen stretching internal coordinates. Thus, the frequency calculated around 1090 cm^{-1} is a stretching mode having CC, CN, and CO characters, while the absorption calculated around 1010 cm^{-1} is a vibration containing a high CO stretching contribution. The corresponding experimental bands are measured at 1088 and 1027 cm^{-1}. Another CO stretching calculated around 1200 cm^{-1} would be associated to the band observed at 1175 cm^{-1}. The experimental band 964 cm^{-1} could be assigned to a CC stretching vibration coupled with the CN one.

The DFT calculations performed on variable-size clusters of methyl ammonium nitrate provide for the splitting of the ν_3 mode of NO_3^- the value 45 cm^{-1} and suggest the effect of complexation to have scarce influence on the other vibrations of the anion.[61] It has to be stated that according to the present computations, the splitting of the ν_3 mode is predicted to be 40 cm^{-1} for the *anti* conformer and lower (13 cm^{-1}) for the *gauche* one for the largest size clusters considered. The two intense bands measured at 1336 and 1382 cm^{-1}, separated by 46 cm^{-1}, both ascribable to the split components of the ν_3 mode, are in agreement with the theoretical expectations reached by other authors for similar variable-size clusters.[59–61] From this observation one would conclude that the liquid might largely consist of *anti* type conformers of the cation. If one compares the value predicted by the cluster calculation with the one predicted by AIMD trajectory analysis (55 cm^{-1}, see Table I), we might conclude that the two methods are substantially in agreement, also considering that the AIMD value refers to a spectrum obtained from the whole collection of trajectory frames.

The consequences of ion-coupling on the ν_1 and ν_2 modes are quite modest: the Raman active ν_1 mode of the free anion, calculated at ~1100 cm^{-1} and measured in aqueous solutions within 1048-1081 cm^{-1},[64] is IR active in the complex and is measured at 1046 cm^{-1}. The out-of-plane deformation mode

(ν_2) of the free anion predicted at ~850 cm^{-1}, and measured within 832-843 cm^{-1}, is present in our infrared spectrum at 825 cm^{-1}. The ν_4 degenerate bending mode, calculated at ~740 cm^{-1}, corresponds to the measured IR band observed at 720 cm^{-1} showing no measurable splitting. The same conclusions reached by us are also experimentally confirmed for crystalline $CH_3NH_3^+NO_3^-$.[65]

IV. CONCLUSIONS

In this work, the comparison between experimental X-ray scattering profiles and infrared spectra and *ab initio* molecular dynamics simulations are reported for the protic ionic liquid 2-OMeEAN. The agreement obtained between experimental and theoretical results is remarkably good and allows us to trace precise structural features of the local liquid structure. In this system, as in many other ionic liquids, the molecules are involved in an extended hydrogen bond network that connects cations and anions. The geometrical parameter obtained for the N···O distance is ~2.8 Å and it is in line with literature values. A linear shape was observed for the hydrogen bond with an angular distribution ranging between 160°and 180°, indicating a rather strong interaction. It was also confirmed that ILs with a polar group in the alkyl chain establish new short intramolecular contacts that lead to the disappearance of the medium-range order, resulting in the absence of the structure function pre-peak. In this particular system the heteroatom of the alkyl chain brings about additional intramolecular interactions that induce a folding of the cation leading to the more stable *gauche* conformer. It is noteworthy to point out how this feature comes out spontaneously without use of restraints or particular choices of the molecular dynamics parameters as seen in previous classical calculation. The infrared spectrum obtained from our simulations is in very good agreement with the experimental pattern, allowing unambiguous identification of several internal vibrational motions. Thanks to the projection of the power spectrum onto collective coordinates, it was possible to distinguish the partial contribution of all the effective normal modes. In the cation, the C–H vibrational motions could be separated from the N–H ones. The latter are characterized by a very broad distribution of states which is a clue of the various hydrogen bonding arrangements sampled during the dynamics of the bulk phase, confirmed by the experimental spectrum that shows a similar behaviour.

Regarding the anion, it was concluded that for all of the possible local environments of the nitrate group, the out-of-plane and the in-plane deformations do not virtually lose their double degeneracy, although the symmetry of the anion is thoroughly reduced in the ion-pair. On the contrary, it was shown that the asymmetric stretching vibration loses its degeneracy and the broad band observed in the experimental IR spectrum is related to the manifold structures of the cation-anion pairs existing in the condensed phase. The asymmetric hydrogen bonding environments provide a physical explanation for these spectral features, which cannot be revealed by *in vacuo* calculations alone. It is worth pointing out how the inhomogeneous environment cannot exclusively be attributed to the asymmetric hydrogen bond pattern, but even the weaker and non-directional interactions that are formed between the oxygen atoms of nitrate and the alkyl chains of cations lead to well defined splitting in the VDOS for the asymmetric stretching.

SUPPLEMENTARY MATERIAL

See supplementary material for [GAFF forcefield parameters and residue/atom types definition, Dihedral Distribution Functions (DDFs)].

ACKNOWLEDGMENTS

The authors are deeply grateful to Pietro Ballone, for his support and for the very helpful discussions and to Professor Ruggero Caminiti (Department of Chemistry, Rome Sapienza University) for providing free computing time on NARTEN Cluster HPC Facility. Financial support of the Scientific Committee of the University of Rome through Grant Nos. C26A13KR5Z, C26A142SCB, and C26H13MNEB and computational support from Cineca (Grant No. IsC11_ESP-IL) and PRACE (Grant No. 2013091962) are also gratefully acknowledged.

[1]J. S. Wilkes, Green Chem. **4**, 73 (2002).
[2]E. W. Castner and J. F. Wishart, J. Chem. Phys. **132**, 120901 (2010).
[3]P. Wasserscheid and W. Keim, Angew. Chem., Int. Ed. **39**, 3772 (2000).
[4]G. J. Kabo, A. V. Blokhin, Y. U. Paulechka, A. G. Kabo, M. P. Shymanovich, and J. W. Magee, J. Chem. Eng. Data **49**, 453 (2004).
[5]M. E. Valkenburg, R. L. Vaughn, M. Williams, and J. S. Wilkes, Thermochim. Acta **425**, 181 (2005).
[6]R. Hayes, G. G. Warr, and R. Atkin, Chem. Rev. **115**, 6357-6426 (2015).
[7]H. Watanabe, H. Doi, S. Saito, M. Matsugami, K. Kanzaki, Y. Kameda, and Y. Umebayashi, J. Mol. Liq. **217**, 35-42 (2016).
[8]P. D'Angelo, A. Zitolo, V. Migliorati, E. Bodo, G. Aquilanti, J. L. Hazemann, D. Testemale, G. Mancini, and R. Caminiti, J. Chem. Phys. **135**, 074505 (2011).
[9]T. L. Greaves and C. J. Drummond, Chem. Rev. **108**, 206 (2008).
[10]K. Fumino, A. Wulf, and R. Ludwig, Angew. Chem., Int. Ed. **48**, 3184 (2009).
[11]K. Fumino, A. Wulf, and R. Ludwig, Phys. Chem. Chem. Phys. **11**, 8790 (2009).
[12]K. Fumino, T. Peppel, M. Geppert-Rybczynska, D. H. Zaitsau, J. K. Lehmann, S. P. Verevkin, M. Kockerling, and R. Ludwig, Phys. Chem. Chem. Phys. **13**, 14064 (2011).
[13]R. Hayes, S. Imberti, G. G. Warr, and R. Atkin, Angew. Chem., Int. Ed. **52**, 4623-4627 (2015).
[14]A. Triolo, O. Russina, R. Caminiti, H. Shirota, H. Y. Lee, C. S. Santos, N. S. Murthy, and E. W. Castner, Jr., Chem. Commun. **48**, 4959 (2012).
[15]V. Vchirawongkwin, C. Kritayakornupong, A. Tongraar, and B. M. Rode, J. Phys. Chem. B **115**, 12527 (2011).
[16]J. Thøgersen, J. Réhault, M. Odelius, T. Ogden, N. K. Jena, S. J. K. Jensen, S. R. Keiding, and J. Helbing, J. Phys. Chem. B **117**, 3376 (2013).
[17]L. Gontrani, E. Bodo, A. Triolo, F. Leonelli, P. D'Angelo, V. Migliorati, and R. Caminiti, J. Phys. Chem. B **116**, 13024 (2012).
[18]E. Bodo, S. Mangialardo, F. Capitani, L. Gontrani, F. Leonelli, and P. Postorino, J. Chem. Phys. **140**, 204503 (2014).
[19]S. Zahn, J. Thar, and B. Kirchner, J. Chem. Phys. **132**, 124506 (2010).
[20]V. R. Albertini, R. Caminiti, F. Cilloco, F. Croce, and C. Sadun, J. Macromol. Sci. B **36**, 221 (1997).
[21]R. Caminiti and V. R. Albertini, Int. Rev. Phys. Chem. **18**, 263 (1999).
[22]R. Caminiti, M. Carbone, G. Mancini, and C. Sadun, J. Mater. Chem. **7**, 1331 (1997).
[23]H. J. C. Berendsen, D. V. D. Spoel, and R. V. Drunen, Comput. Phys. Commun. **91**, 43 (1995).
[24]J. Wang, R. M. Wolf, J. W. Caldwell, P. A. Kollman, and D. A. Case, J. Comput. Chem. **25**, 1157 (2004).

[25]D. A. Case, T. A. Darden, T. E. Cheatham, C. L. Simmerling, J. Wang, R. E. Duke, R. Luo, R. C. Walker, W. Zhang, K. M. Merz, B. Roberts, S. Hayik, A. Roitberg, G. Seabra, J. Swails, A. W. Goetz, I. Kolossváry, K. F. Wong, F. Paesani, J. Vanicek, R. M. Wolf, J. Liu, X. Wu, S. R. Brozell, T. Steinbrecher, H. Gohlke, Q. Cai, X. Ye, J. Wang, M. J. Hsieh, G. Cui, D. R. Roe, D. H. Mathews, M. G. Seetin, R. Salomon-Ferrer, C. Sagui, V. Babin, T. Luchko, S. Gusarov, A. Kovalenko, and P. A. Kollman, AMBER 12, University of California, San Francisco, 2012.
[26]J. Wang, W. Wang, P. A. Kollman, and D. A. Case, J. Mol. Graphics Modell. **25**, 247 (2006).
[27]CP2k version 2.4 (Development Version), the CP2k developers group (2013). CP2k is freely available from: http://www.cp2k.org.
[28]J. VandeVondele, M. Krack, F. Mohamed, M. Parrinello, T. Chassaing, and J. Hutter, Comput. Phys. Commun. **167**, 103 (2005).
[29]J. VandeVondele and J. Hutter, J. Chem. Phys. **118**, 4365 (2003).
[30]P. Hohenberg and W. Kohn, Phys. Rev. **136**, B864 (1964).
[31]W. Kohn and L. J. Sham, Phys. Rev. **140**, A1133 (1965).
[32]J. P. Perdew, K. Burke, and M. Ernzerhof, Phys. Rev. Lett. **77**, 3865 (1996).
[33]S. Grimme, J. Comput. Chem. **27**, 1787 (2006).
[34]J. VandeVondele and J. Hutter, J. Chem. Phys. **127**, 114105 (2007).
[35]S. Goedecker, M. Teter, and J. Hutter, Phys. Rev. B **54**, 1703 (1996).
[36]C. Hartwigsen, S. Goedecker, and J. Hutter, Phys. Rev. B **58**, 3641 (1998).
[37]M. J. Frisch, G. W. Trucks, H. B. Schlegel, G. E. Scuseria, M. A. Robb, J. R. Cheeseman, G. Scalmani, V. Barone, B. Mennucci, G. A. Petersson, H. Nakatsuji, M. Caricato, X. Li, H. P. Hratchian, A. F. Izmaylov, J. Bloino, G. Zheng, J. L. Sonnenberg, M. Hada, M. Ehara, K. Toyota, R. Fukuda, J. Hasegawa, M. Ishida, T. Nakajima, Y. Honda, O. Kitao, H. Nakai, T. Vreven, J. A. Montgomery, Jr., J. E. Peralta, F. Ogliaro, M. Bearpark, J. J. Heyd, E. Brothers, K. N. Kudin, V. N. Staroverov, R. Kobayashi, J. Normand, K. Raghavachari, A. Rendell, J. C. Burant, S. S. Iyengar, J. Tomasi, M. Cossi, N. Rega, J. M. Millam, M. Klene, J. E. Knox, J. B. Cross, V. Bakken, C. Adamo, J. Jaramillo, R. Gomperts, R. E. Stratmann, O. Yazyev, A. J. Austin, R. Cammi, C. Pomelli, J. W. Ochterski, R. L. Martin, K. Morokuma, V. G. Zakrzewski, G. A. Voth, P. Salvador, J. J. Dannenberg, S. Dapprich, A. D. Daniels, Farkas, J. B. Foresman, J. V. Ortiz, J. Cioslowski, and D. J. Fox, Gaussian 09, Revision E.01, Gaussian, Inc. Wallingford, CT, 2009.
[38]A. D. Becke, J. Chem. Phys. **98**, 5648 (1993).
[39]J.-D. Chai and M. Head-Gordon, Phys. Chem. Chem. Phys. **10**, 6615 (2008).
[40]J. Tomasi, B. Mennucci, and R. Cammi, Chem. Rev. **105**, 2999 (2005).
[41]M.-P. Gaigeot, M. Martinez, and R. Vuilleumier, Mol. Phys. **105**, 2857 (2007).
[42]M. Martinez, M.-P. Gaigeot, D. Borgis, and R. Vuilleumier, J. Chem. Phys. **125**, 144106 (2006).
[43]M. Macchiagodena, F. Ramondo, A. Triolo, L. Gontrani, and R. Caminiti, J. Phys. Chem. B **116**, 13448 (2012).
[44]L. Gontrani, O. Russina, F. C. Marincola, and R. Caminiti, J. Chem. Phys. **131**, 244503 (2009).
[45]L. Gontrani, R. Caminiti, L. Bencivenni, and C. Sadun, Chem. Phys. Lett. **301**, 131 (1999).
[46]C. J. Pings and J. Waser, J. Chem. Phys. **48**, 3016 (1968).
[47]X. Song, H. Hamano, B. Minofar, R. Kanzaki, K. Fujii, Y. Kameda, S. Kohara, M. Watanabe, S.-i. Ishiguro, and Y. Umebayashi, J. Phys. Chem. B **116**, 2801 (2012).
[48]H. K. Kashyap, C. S. Santos, R. P. Daly, J. J. Hettige, N. S. Murthy, H. Shirota, J. Edward, W. Castner, and C. J. Margulis, J. Phys. Chem. B **117**, 1130 (2013).
[49]M. Campetella, L. Gontrani, E. Bodo, F. Ceccacci, F. C. Marincola, and R. Caminiti, J. Chem. Phys. **138**, 184506 (2013).
[50]C. Hardacre, J. D. Holbrey, C. L. Mullan, T. G. A. Youngs, and D. T. Bowron, J. Chem. Phys. **133**, 074510 (2010).
[51]D. A. Keen, J. Appl. Cryst. **34**, 172 (2001).
[52]P. G. Kusalik, D. Bergman, and A. Laaksonen, J. Chem. Phys. **113**, 8036 (2000).
[53]M. Brehm and B. Kirchner, J. Chem. Inf. Model. **51**, 2007 (2011).
[54]D. Bovi, A. Mezzetti, R. Vuilleumier, M.-P. Gaigeot, B. Chazallon, R. Spezia, and L. Guidoni, Phys. Chem. Chem. Phys. **13**, 20954 (2011).
[55]D. Bovi, D. Narzi, and L. Guidoni, New J. Phys. **16**, 015020 (2014).
[56]G. Fogarasi, X. Zhou, P. W. Taylor, and P. Pulay, J. Am. Chem. Soc. **114**, 8191 (1992).
[57]P. Niga, D. Wakeham, A. Nelson, G. G. Warr, M. Rutland, and R. Atkin, Langmuir **26**, 8282 (2010).
[58]C. Adamo and V. Barone, J. Chem. Phys. **110**, 6158 (1999).
[59]E. Bodo, P. Postorino, S. Mangialardo, G. Piacente, F. Ramondo, F. Bosi, P. Ballirano, and R. Caminiti, J. Phys. Chem. B **115**, 13149 (2011).
[60]E. Bodo, S. Mangialardo, F. Ramondo, F. Ceccacci, and P. Postorino, J. Phys. Chem. B **116**, 13878 (2012).
[61]L. F. O. Faria, T. C. Penna, and M. C. C. Ribeiro, J. Phys. Chem. B **117**, 10905 (2013).
[62]M. H. Jamróz, Spectrochim. Acta, Part A **114**, 220 (2013).
[63]G. Schaftenaar and J. H. Noordik, J. Comput. Aid. Mol. Des. **14**, 123 (2000).
[64]D. J. Goebbert, E. Garand, T. Wende, R. Bergmann, G. Meijer, K. R. Asmis, and D. M. Neumark, J. Phys. Chem. A **113**, 7584 (2009).
[65]M. Mylrajan and T. K. K. Srinivasan, J. Raman Spectrosc. **16**, 412 (1985).